

Experimental Molecular Communication Testbed Based on Magnetic Nanoparticles in Duct Flow

(Invited Paper)

Harald Unterweger*, Jens Kirchner[†], Wayan Wicke[‡], Arman Ahmadzadeh[‡], Doaa Ahmed[†], Vahid Jamali[‡], Christoph Alexiou*, Georg Fischer[†], and Robert Schober[‡]

*ENT-Department, Section of Experimental Oncology and Nanomedicine (SEON), Universitätsklinikum Erlangen

[†]Institute for Electronics Engineering, Friedrich-Alexander-Universität Erlangen-Nürnberg

[‡]Institute for Digital Communications, Friedrich-Alexander-Universität Erlangen-Nürnberg

Abstract—Simple and easy to implement testbeds are needed to further advance molecular communication research. To this end, this paper presents an in-vessel molecular communication testbed using magnetic nanoparticles dispersed in an aqueous suspension as they are also used for drug targeting in biotechnology. The transmitter is realized by an electronic pump for injection via a Y-connector. A second pump provides a background flow for signal propagation. For signal reception, we employ a susceptometer, an electronic device including a coil, where the magnetic particles move through and generate an electrical signal. We present experimental results for the transmission of a binary sequence and the system response following a single injection. For this flow-driven particle transport, we propose a simple parameterized mathematical model for evaluating the system response.

I. INTRODUCTION

Applications such as drug targeting or monitoring of chemical reactors spurred the interest in and theoretical growth of molecular communication; an approach for communication using small particles in areas impenetrable for electromagnetic waves, see [1] for an overview of the recent literature.

Experimental studies have successfully demonstrated different components of a molecular communication system, see [2]–[6] and references therein. However, realizing a fully-functional artificial molecular communication system at nanoscale remains a challenge. Nevertheless, for first experimental insights, testbeds in the size range of several cm have been proposed. In particular, the system described in [7] is based on spraying and detecting alcohol in open space, and the testbed in [8] is based on signaling with acids and bases for signaling within closed vessels. The testbed in [7] has been extended to a multiple-input and multiple-output (MIMO) system and to a confined environment within a metal pipe [9], [10]. Also, improved theoretical models have been proposed to account for apparent discrepancies between theory and experiment [11].

Considering the potential applications, a testbed using tubes, e.g., for emulating blood vessels, is relevant. On the other hand, using chemicals like acids and bases for information transmission could potentially interfere with other processes in an application environment, e.g., in the body. Furthermore, the detection mechanism in [8] is intrusive as it relies on

a pH-electrode inserted into the vessel. On the other hand, information particles do not have to be restricted to those occurring in nature [1]. One type of artificial particle that is already well-established in biotechnology are biocompatible magnetic nanoparticles [12]. These particles can be tailored to a particular application by engineering of their size, composition, and coating [13]. Moreover, magnetic nanoparticles can be attracted by a magnet and externally visualized, which can help detection and supervision. Applications of magnetic nanoparticles include tissue engineering, biosensing, imaging, remotely stimulating cells, waste-water treatment [14], and drug delivery, see [12] and references therein.

In the context of molecular communication, the use of magnetic nanoparticles has been considered in [15] and [16], where the benefits of attracting them as information carriers towards a receiver are evaluated and a wearable device for detecting the presence of magnetic nanoparticles is proposed, respectively. However, a practical molecular communication testbed employing magnetic nanoparticles has not been reported, yet.

Similar to [8], in this paper, we present a testbed for in-vessel molecular communication. Our setup differs in that it uses specifically designed magnetic nanoparticles as information carriers, which are biocompatible, clinically safe and do not interfere with other chemical processes like acids and bases would do, and thus might be attractive for applications such as the monitoring of chemical reactors where particles stored in a reservoir could be released upon an event like the detection of a defect. Here, magnetic nanoparticles are injected and transported along a propagation tube using two electronic pumps. The propagation tube leads through the receiver where the magnetic susceptibility of the mixture of water and magnetic nanoparticles within a tube section can be non-intrusively determined. The magnetic susceptibility measured at a tube section is proportional to the concentration of the particles within the section. This proportionality lends itself better for mathematical analysis than the pH, which depends on the underlying proton concentration in a more complicated manner [8].

For the chosen parameters, we find laminar flow-driven particle transport applicable for signal propagation after injec-

This work was supported in part by the Emerging Fields Initiative (EFI) of the Friedrich-Alexander-Universität Erlangen-Nürnberg (FAU).

TABLE I
SYSTEM PARAMETERS

Parameter	Numerical Value
Hydrodynamic particle radius	27.5 nm
Suspension iron stock concentration	7.89 mg/mL
Suspension magnetic susceptibility	7.28×10^{-3} (SI units)
Tube radius particle injection	0.40 mm
Tube radius background flow a	0.75 mm
Flow rate particle injection Q_p	5.26 mL/min
Flow rate background flow Q_b	5 mL/min
Volume particle injection V_i	14 μ L
Duration particle injection	160 ms
Binary symbol duration T	4 s
Propagation distance d	5 cm
Receiver length c_z	18 mm
Receiver inner radius a_{RX}	5 mm

tion. We model the injection as being axially concentrated and adhering to a parameterized initial distribution in the cross section at the site of injection. Modeling this transport by neglecting diffusion and assuming a parabolic flow profile yields a good agreement with the experimental results.

The rest of this paper is organized as follows. In Section II, we describe the components of the proposed system and the overall testbed. In Section III, we characterize the expected system response mathematically. In Section IV, we present experimental data and evaluate the theoretical model. Finally, Section V concludes the paper.

II. MAGNETIC NANOPARTICLE BASED TESTBED

In the following, each component of the system is briefly described. A representative photograph of the whole system is shown in Fig. 1a, while Table I summarizes the system parameters.

A. Carrier and Transmitter

In the considered system, superparamagnetic iron oxide nanoparticles (SPIONs), which were originally developed for biomedical applications, are used as information carriers, due to their magnetic properties. In particular, we employed lauric acid coated SPIONs (SPION^{LA}), which were originally developed for magnetic drug targeting purposes [17]. The particles are dispersed in an aqueous suspension and stored in a syringe, which is connected to a tube with an inner radius of 0.4 mm. These particles have a hydrodynamic radius of 27.5 nm, an iron stock concentration of 7.89 mg/mL, a susceptibility of 7.28×10^{-3} (dimensionless in SI units), and a concentration of approximately 4×10^{13} Particles/mL in aqueous suspension. The movement of the particles through the tube is established with a computer controlled peristaltic pump (Ismatec[®] Reglo Digital, Germany), which can provide discrete pumping actions at a flow rate of 5.26 mL/min, injecting a dosage volume of 14 μ L of particle suspension.

The end of the tube with the particles is joined via a Y-connector with another tube of radius 0.75 mm providing a background flow, see Fig. 1b. The constant background flow of water has a flow rate of 5 mL/min and is maintained by a second pump (Ismatec[®] IPC, Germany).

B. Propagation Channel

The Y-connector constitutes the end of the transmitter; its end piece passes into the propagation channel, which also has an inner tube radius of 0.75 mm. The flow rate in this channel is the sum of the rates of the background flow and the particle injection. It is hence time-dependent and amounts to 10.26 mL/min during particle injection and 5 mL/min in the remaining time. When particles are pumped into the channel by the transmitter, then the resulting particle cloud is entrained by the flow and simultaneously diluted and elongated, see Fig. 1b.

The length of the propagation channel is variable, but was set to 5 cm for the results shown.

C. Receiver

At the end of the propagation channel, the tube runs through the air core of an MS2G Bartington[®] susceptometer coil (inner diameter: 10 mm, height: 5 mm). When the magnetic particles are within the detection range of the susceptometer, an electrical signal $\chi(t)$ is generated. This signal is proportional to the number of SPIONs that are within the detection range at a specific time instance. After the particles have passed through the receiver, they are collected in a waste bin together with the water from the background flow. Water has a small negative magnetic susceptibility of about -9.04×10^{-6} (SI units) [18]. However, its magnitude is much less than that of the considered particle suspension $\chi_{ref} = 7.28 \times 10^{-3}$ (SI units).

D. Communication Scheme

Modulation uses on-off keying and is realized by a custom LabVIEW (National Instruments, Austin, Texas, USA) graphical user interface (GUI) that triggers the discrete pumping actions of the particle pump: Every time a binary symbol "1" shall be sent by the transmitter, a dose of particle solution is injected into the propagation channel; if a "0" shall be sent, no particles are injected. From the injection volume and the flow rate in the particle tube, the injection duration is calculated as 160 ms, while the symbol interval was set to 4 s.

For sending a text message, the 8 bit extended ASCII encoding for capital letters is used. The 26 capital letters each have a $[0, 1, 0]$ prefix, which we use for synchronization. In this way, the receiver recognizes the start of a character by the first detected peak position.

The susceptibility changes measured at the receiver were recorded by use of the software Bartsoft 4.2.1.1 (Bartington Instruments, Witney, UK) provided by the manufacturer of the susceptometer. For detection of SPION injections at the receiver, a constant threshold was applied.

Transmission proceeds as follows. For each 8-bit message, the initial peak position t_0 is determined. Then, the following five bits are detected by comparing $\chi(t_0 + T + kT)$, $k = 1, 2, 3, 4, 5$ with a threshold.

III. SYSTEM MODEL

In this section, we develop a simple model for the particle transport in the described testbed. First, we determine characteristic dimensionless parameters relevant for our analysis.

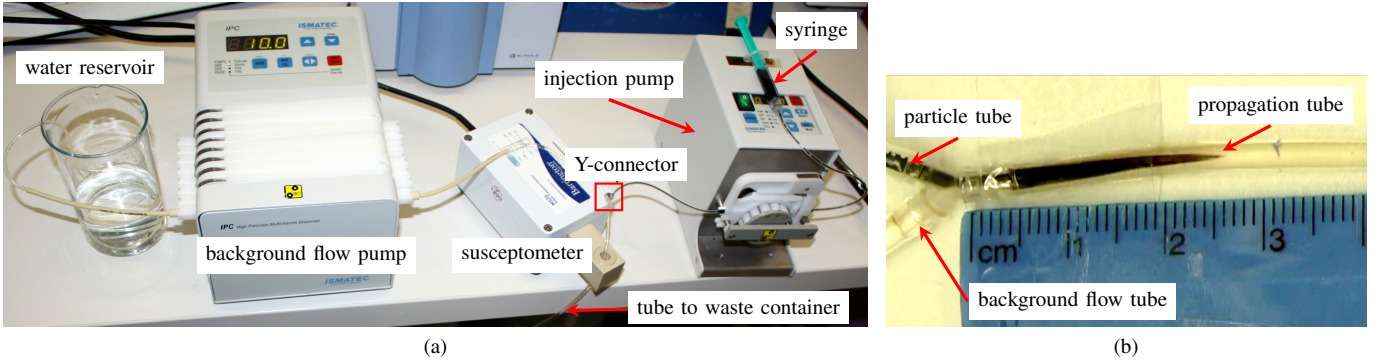


Fig. 1. (a) Photograph of the testbed showing the water reservoir, the background flow pump, the susceptometer, the pump used for injection, the syringe holding the suspension of SPIONs, and flexible plastic tubes connecting the components. The waste container below the table is not shown. (b) Photograph of the Y-connector with elongated particle suspension right after injection for a slow background flow of $Q_b = 1 \text{ mL/min}$. Ruler with cm scale for reference.

Then, we briefly describe the particle transport and give an analytical expression for the expected system response.

A. General Considerations

Fluid flow can be categorized as either laminar or turbulent. This categorization determines the appropriate mathematical model to be used. While laminar flow is prevalent in microfluidic applications, turbulent flows are encountered in macroscale ducts in the size range of several cm. The relevant parameter, in this case, is the Reynolds number Re which predicts a transition from laminar to turbulent flow within a circular duct at a value around 2100, see [18, Chapter 4.10]. Thereby, Re can be defined as [18, Chapter 4.10]

$$Re = \frac{2a \cdot v_{\text{eff}}}{\nu}, \quad (1)$$

where $2a$ is the tube diameter, $v_{\text{eff}} = Q_b/(\pi a^2)$ is the area-averaged velocity in the tube, and ν is the kinematic viscosity of the liquid in m^2/s . For the parameters in Table I, we find $v_{\text{eff}} = 47.2 \text{ mm/s}$. Thus, using the kinematic viscosity of water $\nu = 10^{-6} \text{ m}^2/\text{s}$ [18], we obtain $Re = 70.7 < 2100$ and hence expect fully laminar flow.

For laminar flow in a straight tube of circular cross section, the non-uniform flow velocity profile is well known to be [18]

$$v(r) = v_0 \cdot \left(1 - \frac{r^2}{a^2}\right), \quad (2)$$

where v_0 is the velocity in the center of the tube. For this velocity profile, the area-averaged velocity v_{eff} can be obtained as $v_{\text{eff}} = v_0/2$. In our testbed, the tube is not fully straight. Nevertheless, as the deviations over regular distances on the order of the inner tube diameter are small, the flow profile (2) can be assumed to be a valid approximation.

In general, the particle transport is governed by both diffusion and the fluid flow described in (2). The relative importance of diffusion over the transport by fluid flow considering a distance of d can be quantified by the Péclet number Pe . When $Pe \gg d/a$ and $Pe \ll d/a$, flow and diffusion dominate the transport, respectively. Thereby, Pe can be defined as [19, Eq. (4.6.8)]

$$Pe = \frac{a \cdot v_{\text{eff}}}{D}, \quad (3)$$

where D is the diffusion coefficient of the magnetic particles and can be estimated to be less than $10^{-11} \text{ m}^2/\text{s}$ for the considered SPIONs. Hence, for the parameters in Table I, we obtain $Pe > 3.54 \times 10^6$. This value is several orders of magnitude larger than $d/a = 66.7$ and therefore the impact of diffusion is assumed to be negligible over the considered distance d [19].

Motivated by this dimensional analysis, for simplicity, we will assume the transport can be described only by the velocity profile in (2), see also the shape of the propagating SPION cloud in Fig. 1b.

B. Mathematical Model

The flow at the injection site is complicated as highlighted in Section II-B. Nevertheless, right after the injection pump stops pumping, the resulting volume distribution completely determines the received signal via the laminar flow in (2). For example, when due to the injection more particles are concentrated along the axis than on the boundary of the tube, a faster decay of the received signal and a larger peak can be expected. In fact, in our experiments, we observed varying decay profiles of the received signal depending on the choice of parameters. Hence, we are interested in developing a model for the initial volume distribution. To this end, we note that regarding the received signal, the injected volume distribution is not unique. In fact, due to the radially symmetric flow profile and the receiver covering the whole cross section of the tube, for any non-symmetric volume distribution there is always an equivalent radially symmetric volume distribution resulting in the same received signal. Moreover, as first order approximation, we will assume that the initial distribution can be modeled as being axially concentrated at the site of injection as the time of injection is short compared to the symbol duration. Then, for choosing this initial distribution, we have the following requirements. First, it should have a parameter which can be tuned to the application scenario. Second, it should lead to a simple model for the received signal while providing a good fit to the experimentally observed data. We note that a more accurate model could be obtained, for example, by numerical simulation and evaluating the obtained initial volume distribution. As this numerical simulation does

not directly give theoretical insight, in this paper, we will focus on the transport by the laminar flow (2) and leave a more careful study of the injection process for future work.

Two common models for introducing particles in a straight tube are uniformly over the inlet cross section or in a concentration proportional to the velocity profile in (2) [20, Chapter 15]. This leads to observed particle concentrations at the outlet with decays proportional to powers of $1/t$ [20, Chapter 15]. Motivated by our experimental observation of varying decays of the received signal and the considerations above, we consider the following example initial SPION distribution over the cross section at the axial position of the injection

$$f_{x,y}(x, y) = \frac{\beta + 1}{\pi a^2} \cdot \left(1 - \frac{x^2 + y^2}{a^2}\right)^\beta, \quad (4)$$

where $\beta \geq 0$ is a shape parameter and the Cartesian coordinates x, y satisfy $x^2 + y^2 \leq a^2$. For $\beta = 0$, we obtain a uniform initial distribution $f_{x,y}(x, y) = 1/(\pi a^2)$ over the cross section. For $\beta \rightarrow \infty$, we obtain $f_{x,y}(x, y) = \delta(x)\delta(y)$ where all particles are concentrated in the center of the tube. In general, the larger β , the more particles are initially centered in the tube.

By the methodology in [21], with (4) we obtain the system response as

$$P_{\text{ob}}(t) = \begin{cases} 0, & t \leq \frac{d}{v_0} \\ 1 - \left(\frac{d}{v_0 t}\right)^{\beta+1}, & \frac{d}{v_0} < t < \frac{d + c_z}{v_0} \\ \frac{(d + c_z)^{\beta+1} - d^{\beta+1}}{(v_0 t)^{\beta+1}}, & t \geq \frac{d + c_z}{v_0} \end{cases} \quad (5)$$

which has a peak of height $1 - (1 + c_z/d)^{-1-\beta}$ for $t_{\text{peak}} = (d + c_z)/v_0$. From the fit of (5) to experimental results, we can infer the value of β and the initial release distribution. From (5), we obtain the expected susceptibility over time as

$$\chi(t) = \chi_{\text{ref}} \frac{V_i}{V_{\text{RX}}} P_{\text{ob}}(t), \quad (6)$$

where χ_{ref} and V_i can be found in Table I and V_{RX} is the volume of the susceptometer's sensitive region which can be obtained as $V_{\text{RX}} = c_z \pi a_{\text{RX}}^2$, where a_{RX} and c_z are the radius and the length of the receiver coil, respectively.

IV. EXPERIMENTAL CHARACTERIZATION

In this section, we present some experimental results obtained with the testbed and numerically evaluate the analytical model proposed in Section III. In the following, the parameters in Section II apply unless specifically indicated otherwise.

In Fig. 2, we show the measured received susceptibility time signal for the example bit sequence $[0, 1, 0, 0, 0, 1, 1, 0, 0, 1, 0, 0, 0, 0, 0, 1, 0, 1, 0, 1, 0, 1, 0, 1]$ encoding 3 characters as described in Section II-D. We also show the decoded bit sequence and the corresponding sampling times. The threshold used for detection is set to $\chi_0 = 1.75 \times 10^{-4}$ and shown as horizontal black line. Furthermore, the peaks used for synchronization, which occur

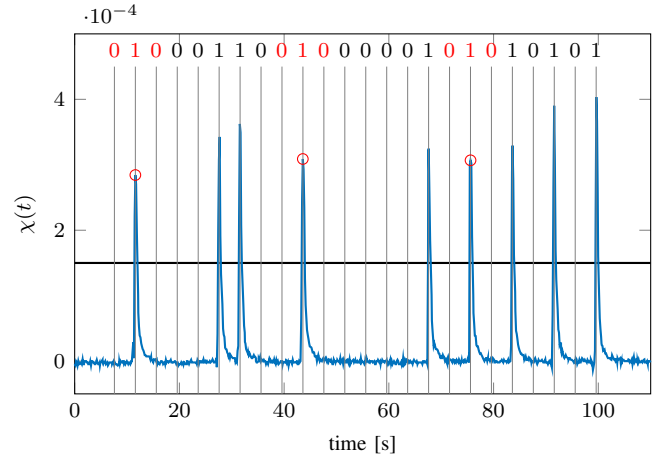


Fig. 2. Example received signal for the bit sequence $[0, 1, 0, 0, 0, 1, 1, 0, 0, 1, 0, 0, 0, 0, 1, 0, 1, 0, 1, 0, 1, 0, 1]$.

at regular distances of $8T$ after the first peak, are marked with red circles. Thereby, the very first peak around 17s was found numerically by analyzing the whole received signal after the transmission of all bits. In particular, all subsequent sampling times are shown by vertical subdued black lines. The shown decoded bits evaluate to 1 and 0 if the received signal at the sampling times is above or below the threshold, respectively. Comparing with the transmitted sequence, we observe that the transmitted sequence is perfectly recovered. In fact, the received signal follows a straightforward pattern, where no pulses are observed when a 0 was transmitted. In other words, there is negligible intersymbol interference. The measurement noise is more than 10 times smaller than the minimum observed peak and thus there is no significant distortion. Considering the injected volume per bit of $14 \mu\text{L}$ and the stored volume of several mL in the syringe, several thousands of consecutive transmissions can be realized without refilling. We also observe small variations in the amplitude of the peaks. These can presumably be attributed to the expected variations of the volume injected by the peristaltic pump which mechanically compresses the particle injection tube. On the other hand, the overall shape of the pulses is not affected by these variations.

In Fig. 3, we show the measured susceptibility over time following a single injection. We consider variations from the baseline parameters in Section II regarding the injection flow rate Q_p , the background flow rate Q_b , and the volume of the injected particle suspension V_i as is also indicated in the figure. Furthermore, we show the analytical solution $\chi(t)$ in (6), where the shape parameter β was numerically found by least-squares fitting to the measured data after time-shifting of the data such that the peaks of the measurement and of the analytical solution align. For a better visualization, the curves are separated by 2s each. For all curves, we can observe a fast increase of the signal from $\chi = 0$ to the peak value and a relatively slower decrease from the peak value back to $\chi = 0$. This behavior is also seen in the fitted analytical curve, which overall agrees reasonably well with the data. Decreasing Q_p to 1.4 mL/min

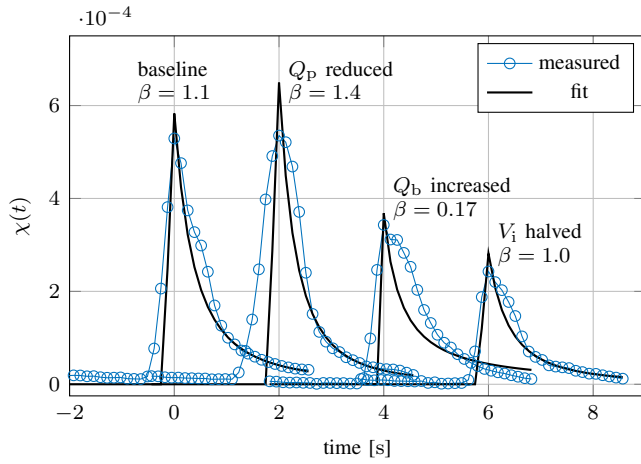


Fig. 3. System response with fit according to (6). For the baseline values, $Q_p = 5.26$ mL/min, $Q_b = 5$ mL/min, and $V_i = 14$ μ L. Following baseline variations are considered. Q_p reduced to 1.4 mL/min, Q_b increased to 10 mL/min, and V_i halved to 7 μ L. Experimental data was averaged over four consecutive pulses.

approximately preserves the amplitude of the pulse and also the decay after the peak with respect to the baseline value. Correspondingly, the value $\beta = 1.1$ of the fitted curve is similar to the baseline value $\beta = 1.4$. For times smaller than the peak time, the pulse is broader compared to the baseline value which is not captured by the analytical curve. This can be explained by our modeling assumption of an axially concentrated release from the cross section which does not strictly hold. Changing Q_b to a larger value of 10 mL/min, leads to a slower decay compared to the baseline scheme. In this case, also the fit parameter is decreased from $\beta = 1.1$ to $\beta = 0.17$ which might be explained as follows. When the background flow becomes stronger, during the injection duration, particles are transported away faster and might not reach the center of the tube where the velocity would be faster compared to when the background flow is slower. Hence, more particles move with slower velocity and thus the measured signal decays slower. When halving V_i to 7 μ L, the received signal is also approximately halved. In this case, the initial release pattern is not yet heavily influenced by the reduction of V_i and parameter $\beta = 1.0$ has a similar value as the baseline $\beta = 1.1$.

V. CONCLUSION

We presented a new testbed for the investigation of molecular communications using the passive detection of engineered magnetic nanoparticles. The proposed system enabled reliable communication, and the measurement of the magnetic susceptibility as a quantity proportional to the particle concentration allowed for a simple mathematical model based on laminar flow-driven particle transport. Potential applications of magnetic nanoparticle based molecular communication include reporting sensing results and carrying control information in industrial, microfluidic or biomedical settings, especially at locations, where other forms of communication could not be employed. The testbed could potentially be expanded by implementing a network of ducts, changing the carrier liquid, or scaling of its

size. Moreover, particles could be additionally tagged with other chemicals. This would, for example, allow for distinguishing releases from different locations or for detecting which kind of event caused a release.

REFERENCES

- [1] N. Farsad, H. B. Yilmaz, A. Eckford, C.-B. Chae, and W. Guo, "A comprehensive survey of recent advancements in molecular communication," *IEEE Commun. Surv. Tutorials*, vol. 18, no. 3, pp. 1887–1919, 2016.
- [2] B. Krishnaswamy, C. M. Austin, J. P. Bardill, D. Russakow, G. L. Holst, B. K. Hammer, C. R. Forest, and R. Sivakumar, "Time-elapse communication: bacterial communication on a microfluidic chip," *IEEE Trans. Commun.*, vol. 61, no. 12, pp. 5139–5151, 2013.
- [3] T. Nakano, Y.-H. Hsu, W. C. Tang, T. Suda, D. Lin, T. Koujin, T. Haraguchi, and Y. Hiraoka, "Microplatform for intercellular communication," in *Proc. IEEE NEMS*, 2008, pp. 476–479.
- [4] T. Nakano, Y. Okaie, S. Kobayashi, T. Koujin, C.-H. Chan, Y.-H. Hsu, T. Obuchi, T. Hara, Y. Hiraoka, and T. Haraguchi, "Performance evaluation of leader–follower-based mobile molecular communication networks for target detection applications," *IEEE Trans. Commun.*, vol. 65, no. 2, pp. 663–676, 2017.
- [5] L. Felicetti, M. Femminella, G. Reali, P. Gesele, M. Malvestiti, and J. N. Daigle, "Modeling CD40-based molecular communications in blood vessels," *IEEE Trans. Nanobioscience*, vol. 13, no. 3, pp. 230–243, 2014.
- [6] N. A. Abbasi, D. Lafci, and O. B. Akan, "Controlled information transfer through an in vivo nervous system," *Sci. Rep.*, vol. 8, no. 1, p. 2298, 2018.
- [7] N. Farsad, W. Guo, and A. W. Eckford, "Tabletop molecular communication: Text messages through chemical signals," *PLoS One*, vol. 8, no. 12, p. e82935, 2013.
- [8] N. Farsad, D. Pan, and A. Goldsmith, "A novel experimental platform for in-vessel multi-chemical molecular communications," in *Proc. IEEE Globecom*, 2017.
- [9] B.-H. Koo, C. Lee, H. B. Yilmaz, N. Farsad, A. Eckford, and C.-B. Chae, "Molecular MIMO: From theory to prototype," *IEEE J. Sel. Areas Commun.*, vol. 34, no. 3, pp. 600–614, 2016.
- [10] S. Qiu, W. Guo, S. Wang, N. Farsad, and A. Eckford, "A molecular communication link for monitoring in confined environments," in *Proc. IEEE ICC*. IEEE, 2014, pp. 718–723.
- [11] N. Farsad, N.-R. Kim, A. W. Eckford, and C.-B. Chae, "Channel and noise models for nonlinear molecular communication systems," *IEEE J. Sel. Areas Commun.*, vol. 32, no. 12, pp. 2392–2401, 2014.
- [12] Q. A. Pankhurst, J. Connolly, S. Jones, and J. Dobson, "Applications of magnetic nanoparticles in biomedicine," *J. Phys. D: Appl. Phys.*, vol. 36, no. 13, p. R167, 2003.
- [13] A.-H. Lu, E. Salabas, and F. Schüth, "Magnetic nanoparticles: synthesis, protection, functionalization, and application," *Angew. Chem. Int. Ed.*, vol. 46, no. 8, pp. 1222–1244, 2007.
- [14] K. G. Raj and P. A. Joy, "Coconut shell based activated carbon–iron oxide magnetic nanocomposite for fast and efficient removal of oil spills," *J. Environ. Chem. Eng.*, vol. 3, no. 3, pp. 2068–2075, 2015.
- [15] W. Wicke, A. Ahmadzadeh, V. Jamali, H. Unterweger, C. Alexiou, and R. Schober, "Molecular communication using magnetic nanoparticles," to be presented at *IEEE WCNC*, 2018. [Online]. Available: <https://arxiv.org/abs/1704.04206>
- [16] S. Kisseleff, R. Schober, and W. H. Gerstacker, "Magnetic nanoparticle based interface for molecular communication systems," *IEEE Commun. Lett.*, vol. 21, no. 2, pp. 258–261, 2017.
- [17] J. Zaloga, C. Janko, J. Nowak, J. Matuszak, S. Knaup, D. Eberbeck, R. Tietze, H. Unterweger, R. P. Friedrich, S. Duerr *et al.*, "Development of a lauric acid/albumin hybrid iron oxide nanoparticle system with improved biocompatibility," *Int. J. Nanomed.*, vol. 9, p. 4847, 2014.
- [18] F. M. White, *Fluid mechanics*, 7th ed. McGraw Hill, 2010.
- [19] R. F. Probstein, *Physicochemical hydrodynamics*. John Wiley & Sons, 2005.
- [20] O. Levenspiel, *Chemical reaction engineering*, 3rd ed. John Wiley & Sons, 1999.
- [21] W. Wicke, T. Schwering, A. Ahmadzadeh, V. Jamali, A. Noel, and R. Schober, "Modeling duct flow for molecular communication," *arXiv preprint arXiv:1711.01479*, 2017.